



# Liver-specific transgenic expression of human NTCP in rhesus macaques confers HBV susceptibility on primary hepatocytes

Lauren N. Rust<sup>a,1</sup> , Jochen M. Wettengel<sup>a,b,c,1</sup> , Sreya Biswas<sup>a</sup>, Junghyun Ryu<sup>d</sup> , Nadine Piekarski<sup>d</sup> , Sofiya Yusova<sup>a</sup>, Savannah S. Lutz<sup>a</sup> , Spandana Naldiga<sup>a</sup>, Brayden J. Hinrichs<sup>a</sup>, Michelle N. Sullivan<sup>e</sup>, Jamie O. Lo<sup>d</sup> , Ulrike Protzer<sup>b,c</sup> , Jeremy V. Smedley<sup>a</sup> , Jonah B. Sacha<sup>a</sup> , Carol B. Hanna<sup>d</sup> , Benjamin N. Bimber<sup>f</sup> , Jon D. Hennebold<sup>d</sup> , and Benjamin J. Burwitz<sup>a,g,2</sup>

Affiliations are included on p. 9.

Edited by Xiang-Jin Meng, Virginia Polytechnic Institute and State University, Blacksburg, VA; received July 11, 2024; accepted December 17, 2024

Hepatitis B virus (HBV) poses a significant global health challenge, necessitating the urgent development of curative therapeutics. However, this progress is impeded by the lack of robust, immunocompetent preclinical animal models due to HBV's strict species specificity. We previously showed that vector-mediated expression of the HBV entry receptor, human sodium-taurocholate cotransporting polypeptide (hNTCP), renders macaques fully susceptible to HBV infection. In this study, we have generated transgenic macaques expressing hNTCP, marking the creation of the first transgenic nonhuman primate model for infectious disease research. We used PiggyBac (PB) transposon technology to insert a liver-specific hNTCP expression cassette into rhesus macaque zygotes and transferred the resulting embryos into surrogate females, resulting in two healthy transgenic offspring. In both animals, hNTCP is highly and selectively expressed in the liver. Most importantly, we show that isolated hepatocytes from these monkeys are susceptible to HBV infection. These findings lay the foundation for the development of a nonhuman primate HBV model, facilitating the advancement and validation of curative HBV therapies.

transgenic | hepatitis B | nonhuman primate | translational model

Transgenic animal models have contributed substantially to our understanding of developmental and cellular biology (1–3). Humans and nonhuman primates share similar reproductive physiology, and a recent spate of reports has helped define the difficulties in engineering specific changes in primate embryonic genomes (4–6). Most of these studies utilized CRISPR/Cas transfection or lentiviral transduction of preimplantation embryos to generate transgenic offspring (7–19). While CRISPR/Cas allows for cutting DNA at a specific locus, gene knock-in is particularly difficult given the extremely low efficiency of homology directed DNA repair, particularly for large inserts (20). In contrast, lentiviral vectors can efficiently integrate up to 8 kilobases of DNA cargo, but the genomic locations of insertions are random. A major barrier to using lentiviral vectors is the creation of lentiviral stocks of sufficient purity and titer to ensure embryo transduction, which also comes at a significant cost and requires technical expertise. Therefore, cheaper and less prohibitive means of rapidly generating knock-in nonhuman primates would accelerate the generation of preclinical models.

Transposon-transposase systems like PiggyBac (PB), Sleeping Beauty, and Tol2 have no cargo limit, lead to random insertion(s) in the genome and mitigate the need to generate ultrahigh titer lentiviral vectors (21). The PB system has been used previously to create transgenic mice, rats, and pigs, although the transgenesis of these species was performed by PB editing of stem cells followed by nuclear transfer (22, 23). Here, we show that the injection of zygotes with a DNA plasmid encoding a tissue-specific expression cassette flanked by PB inverted terminal repeats, together with PB mRNA, leads to the integration of a gene of interest into the genome of rhesus macaques. We use this technology to address a critical gap in HBV research—the current lack of a translational nonhuman primate model of infection.

The World Health Organization estimates that 254 million people are living with chronic hepatitis B infection (CHB) (24), a condition that significantly increases the risk of cirrhosis and hepatocellular carcinoma. Currently available treatments for CHB are limited to nucleos(t)ide analogs and pegylated interferon- $\alpha$ , but nucleos(t)ide analogs must be continued indefinitely, and pegylated interferon- $\alpha$  has significant side effects and multiple contraindications (25, 26). In addition, these therapies rarely lead to a functional cure. Thus, there is a critical need to continue developing and testing curative treatments for CHB.

HBV research is impeded by the absence of a translational, immunocompetent, preclinical in vivo model. Rhesus macaques are the gold standard in vivo model for translational medical research in many infectious disease fields. However, a single amino acid

## Significance

Infectious diseases are often species specific and difficult to model. However, with current genome editing technologies, we can tailor laboratory species for specific research applications. This work addresses a major barrier in the hepatitis B virus (HBV) research field: the lack of a translational, immunocompetent nonhuman primate model. We employed gene editing technology to insert the HBV entry receptor into the genomes of rhesus macaque embryos under a liver-specific promoter, resulting in two healthy transgenic animals. These animals express the HBV entry receptor in their livers with minimal expression in other tissues, and their primary hepatocytes (PH) are susceptible to HBV infection. These animals bridge the gap between emerging therapeutics and a physiological relevant animal for HBV research.

Author contributions: L.N.R., J.M.W., S.N., J.V.S., J.B.S., B.N.B., J.D.H., and B.J.B. designed research; L.N.R., S.B., J.R., N.P., S.Y., S.S.L., S.N., B.J.H., M.N.S., J.O.L., J.V.S., C.B.H., B.N.B., and B.J.B. performed research; U.P. contributed new reagents/analytic tools; L.N.R., S.B., S.N., J.S., B.N.B., and B.J.B. analyzed data; and L.N.R., J.M.W., B.N.B., J.D.H., and B.J.B. wrote the paper.

The authors declare no competing interest.

This article is a PNAS Direct Submission.

Copyright © 2025 the Author(s). Published by PNAS. This article is distributed under [Creative Commons Attribution-NonCommercial-NoDerivatives License 4.0 \(CC BY-NC-ND\)](https://creativecommons.org/licenses/by-nc-nd/4.0/).

<sup>1</sup>L.N.R. and J.M.W. contributed equally to this work.

<sup>2</sup>To whom correspondence may be addressed. Email: burwitz@ohsu.edu.

This article contains supporting information online at <https://www.pnas.org/lookup/suppl/doi:10.1073/pnas.2413771122/-/DCSupplemental>.

Published February 12, 2025.

difference in the HBV entry receptor, human sodium-taurocholate cotransporting polypeptide (hNTCP), renders these animals non-susceptible to HBV infection (27). Our group has demonstrated that adenovirus-mediated expression of hNTCP on hepatocytes renders macaques fully susceptible to in vivo HBV infection (28). This includes the formation of HBV covalently closed circular DNA (cccDNA) in the nucleus, which serves as the viral reservoir that must be eliminated to achieve a functional HBV cure (28, 29).

While this model allows for the study of HBV infection in rhesus macaques, adenovirus-mediated expression of hNTCP has several limitations: i) adenovirus is immunogenic, ii) not all hepatocytes are transduced, and iii) the adenoviral genome and hNTCP expression can be lost during cell division. Therefore, an optimal rhesus macaque HBV model would have transgenic, hepatocyte-specific hNTCP expression to overcome these challenges.

Here, we describe the generation and analyses of two transgenic rhesus macaques with liver-specific hNTCP expression. Our findings demonstrate that these animals remain healthy and selectively express hNTCP in their livers. Most importantly, isolated primary hepatocytes (PH) are susceptible to HBV infection. This unique

animal model is emerging at a critical juncture in HBV research, given the expanded development of curative therapeutics and the lack of immunocompetent models for testing.

## Results

**Design and Testing of hNTCP-Expressing PB Transposon.** We cloned a codon-optimized hNTCP open reading frame under the hepatocyte-specific transthyretin (TTR) promoter into a plasmid encoding core insulator sequences flanked by PB inverted terminal repeats (Fig. 1A). To validate the liver-specific expression of our construct, we transfected this vector in combination with a plasmid expressing PB transposase and GFP into the following cell lines from different species and tissues: HEK293A (human embryonic kidney), CMMT (rhesus macaque mammary epithelial), Vero (vervet kidney epithelial), and Huh7.5 (human hepatocellular carcinoma). We then stained the transfected cell lines with AlexaFluor594-labeled Myrcludex B (MyrB), an HBV pre-S1 derived peptide that binds selectively and with high affinity to hNTCP. We detected cell surface hNTCP expression by FACS

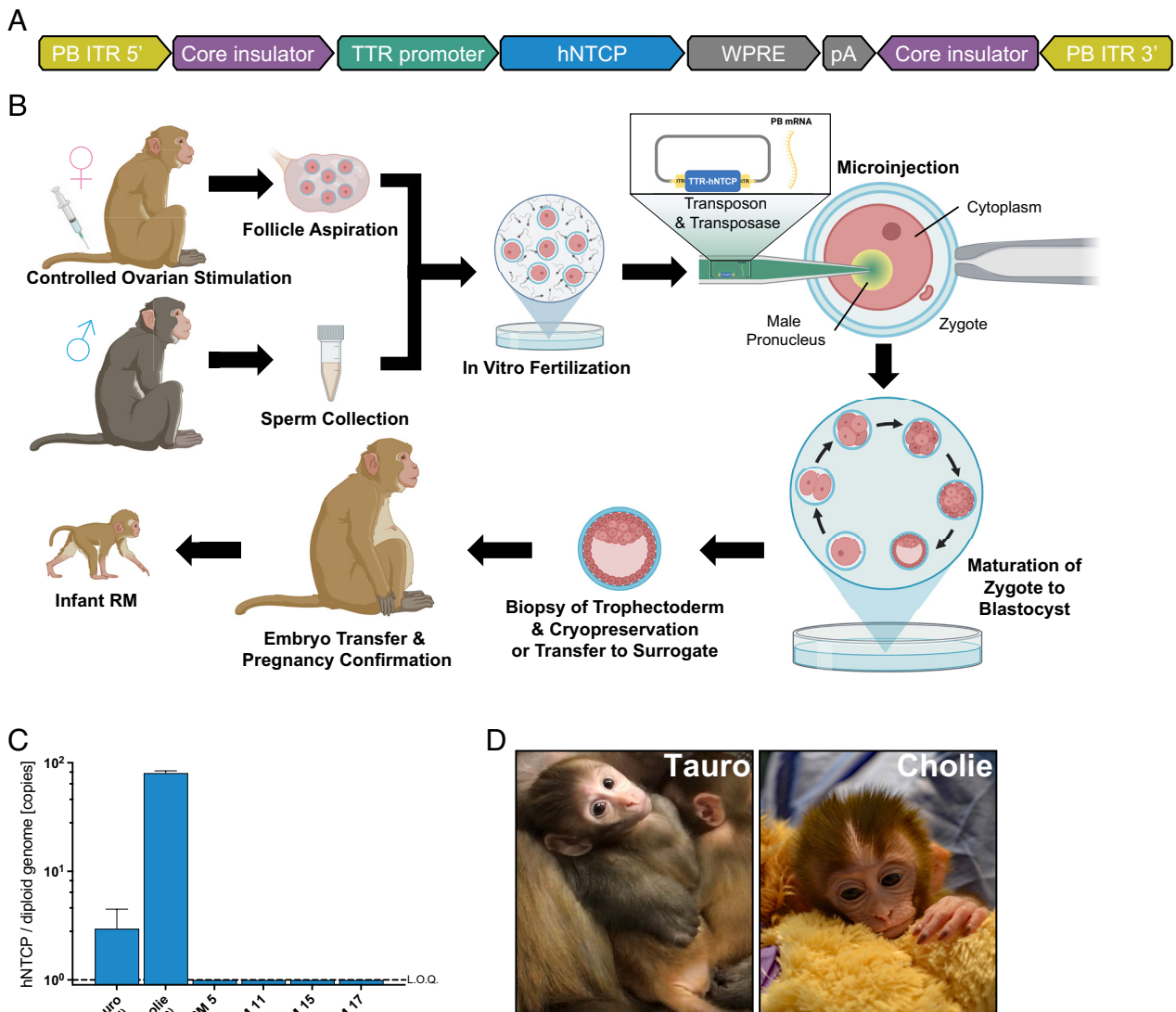


**Fig. 1.** Generation of hNTCP transgenic rhesus macaques. (A) PB transposon encoding TTR-hNTCP used to generate transgenic rhesus macaques. (B) Schema for in vitro fertilization (IVF), microinjection of PB transposon, and embryo transfer to surrogate rhesus macaques. (C) hNTCP DNA quantification in the blood of Tauro (RM 4) and Cholie (RM 20) compared to four nontransgenic animals. (D) Photos of infants Tauro and Cholie. PB = PiggyBac, ITR = inverted terminal repeat sequence, TTR = transthyretin promoter, hNTCP = human sodium taurocholate cotransporting polypeptide, WPRE = woodchuck post-translational response element, pA = polyadenylation signal. Created in BioRender. Rust, L. (2025) <https://BioRender.com/m05s754>.

only on Huh7.5 cells, confirming the hepatocyte specificity of the TTR promoter-driven expression cassette (*SI Appendix, Fig. S1*). Next, we extracted genomic DNA and used our recently published esTag-PCR (30) to confirm PB integration of the TTR-hNTCP cassette into the genomes of the transfected cell lines. As expected, we found PB-mediated integration of the TTR-hNTCP expression cassette in all cell lines. Thus, our PB transposon facilitated genomic integration and hepatocyte-specific hNTCP expression.

**Generation of hNTCP Transgenic Rhesus Macaques.** Having confirmed the functionality and specificity of our hNTCP expression cassette, we next set out to create transgenic rhesus macaques expressing hNTCP. We performed controlled ovarian stimulations on sexually mature, cycling female rhesus macaques within four days of the onset of menses. Mature, metaphase II (MII) ova were recovered from preovulatory follicles by percutaneous ultrasound-guided or laparoscopic aspiration (Fig. 1*B*). From these stimulations, we collected 145 oocytes and sorted them according to their stage of meiosis (Germinal Vesicle: 15, Metaphase II: 94, Metaphase I: 24). In vitro fertilization (IVF) was performed using freshly collected sperm from sexually mature male rhesus macaques. We confirmed fertilization by the presence of either two polar bodies or two pronuclei, and the presumed zygotes were microinjected in both the pronuclei and cytoplasm with PB mRNA and our donor plasmid containing the hNTCP-expressing PB transposon. Injected embryos were cultured to the morula or blastocyst stage and either transferred directly into timed female recipients or trophectoderm cells were biopsied for genetic analysis prior to vitrification. We transferred a total of 34 embryos (fresh  $n = 18$ , frozen  $n = 16$ ) across 21 transfers (fresh  $n = 10$ , frozen  $n = 11$ ) to 17 surrogate females, resulting in seven pregnancies (six singletons and one twin) confirmed by ultrasound examination (Table 1). One of these embryos was confirmed edited by trophectoderm esTag-PCR prior to vitrification and resulted in a successful pregnancy (Table 2). Six healthy infants were born (one singleton pregnancy resulted in a nontransgenic stillbirth (RM 7) at 20 wk gestation, and one singleton pregnancy resulted in spontaneous abortion (RM 24) at 7 wk gestation).

**Characterization of hNTCP Integration and Expression.** We analyzed blood from the six healthy rhesus macaque infants to test for genomic integration of our hNTCP-expressing PB transposon. Using a sensitive qPCR assay that distinguishes hNTCP from the endogenous rhesus macaque NTCP (29), we found the presence of hNTCP in the genomic DNA of two of the six animals (RM 4 and RM 20; Fig. 1 *C* and *D*). We named these transgenic animals Tauro (RM 4) and Cholie (RM 20) in recognition of the transgene they

carry. To further validate these results, we obtained biopsies from liver, skin, axillary lymph node, muscle, and rectum from each infant and isolated both DNA and RNA. While all tissue biopsies collected from Tauro and Cholie showed genomic integration of the PB transposon by qPCR (Fig. 2*A*), only the liver sample exhibited high transcription of hNTCP RNA (Fig. 2*B*), validating the *in vivo* liver-specificity of the TTR promoter-driven expression cassette. In addition, the level of hNTCP expression in Tauro and Cholie was comparable to human PH (Fig. 2*B*). We found that Cholie exhibited higher copy numbers of hNTCP in both DNA and RNA, indicating she potentially harbored a greater number of expressed PB transposon integrations than Tauro. Therefore, we next set out to determine the number and locations of PB transposon integrations in the genomes of Tauro and Cholie.

**Identification of PB Transposon Genomic Integration Sites.** We used esTag-PCR to amplify and deep sequence integration sites in the DNA of biopsied tissues collected from Tauro and Cholie. This analysis indicated a single PB transposon integration in the genome of Tauro and 19 in the genome of Cholie (Table 2). All integration sites were further analyzed by PCR and Sanger sequencing of the genome:transposon junctions, confirming the single integration site for Tauro, and 17 of the 19 for Cholie (*SI Appendix, Table S1*). Interestingly, we only confirmed six integration sites identified by esTag-PCR in Cholie's trophectoderm biopsy (Table 2 and *SI Appendix, Fig. S2*). This disparity in the number and location of integrations found in these sample types may be due to the low quality of DNA or presence of certain integrations only in the trophectoderm. Notably, the same integrants were found in each biopsied tissue from Cholie and Tauro via esTag-PCR (Table 2). However, for both animals, we cannot exclude the possibility of mosaicism without single-cell DNA analyses.

**Clinical Measurements.** Tauro and Cholie were born via vaginal delivery with appropriate growth and behavioral development. All physical exam parameters and laboratory tests were within normal limits, and routine complete blood counts and serum chemistry panels for both animals were clinically unremarkable. Mild to moderate elevations in alkaline phosphatase (190 to 1002 IU/L, normal range 114 to 482 IU/L) and mild elevations in gamma-glutamyl transferase (45 to 134 IU/L, normal range 35 to 72 IU/L) were observed, which are considered normal in young, growing rhesus macaques and not clinically significant (Table 3). Minor intermittent increases in aspartate transaminase (48 to 66 IU/L, normal 18 to 58 IU/L) also occurred; however, many physiologic sources for this enzyme and minor elevations are not considered clinically significant. Primary measures of hepatocyte

**Table 1. Donor animal IDs, in vitro fertilization (IVF) cycling, and pregnancy information for transgenic rhesus macaque generation**

Egg donor ID	Sperm donor ID	Surrogate ID	Fresh/frozen	# Embryos transferred	Embryo stage	Embryo day	Offspring ID	Offspring sex	Transgene identified?
RM 1	RM 2	RM 3	Fresh	2	Blast (2)	6	RM 4 RM 5	Male Female	Yes No
RM 1	RM 2	RM 6	Fresh	2	ExB/H, ExB	7	RM 7*	Male	No
RM 8	RM 9	RM 10	Fresh	2	M (2)	5	RM 11	Male	No
RM 12	RM 13	RM 14	Fresh	2	M, EB	6	RM 15	Female	No
RM 12	RM 13	RM 16	Fresh	2	M (2)	7	RM 17	Female	No
RM 1	RM 18	RM 19	Frozen	1	ExB	7	RM 20	Female	Yes
RM 12, RM 21	RM 22	RM 23	Frozen	2	Blast (2)	7	RM 24*	N/A	N/A

RM = rhesus macaque, Blast = blastocyst, ExB/H = Expanded hatching blastocyst, M = morula, ExB = expanding blastocyst, \* = unsuccessful pregnancy.

**Table 2. Identification of PB transposon genomic integration sites in Tauro and Cholie by esTag-PCR**

Animal ID	Chromosome	Position	Strand	Biopsy sample type
Tauro	5	134932438	+	Tissue (5/5)*
Cholie	2	71880972	-	Trophectoderm
	3	86696258	+	Tissue (5/5)
	3	100887142	-	Tissue (5/5), Trophectoderm
	5	28585155	-	Tissue (5/5), Trophectoderm
	5	134932431	+	Tissue (5/5)
	6	63213830	+	Tissue (5/5)
	6	75218312	+	Trophectoderm
	6	80529947	-	Tissue (5/5), Trophectoderm
	6	80631153	-	Tissue (5/5)
	6	169318101	+	Trophectoderm
	7	32035790	-	Trophectoderm
	7	85409662	-	Tissue (5/5)
	8	78014366	+	Tissue (5/5), Trophectoderm
	9	109238848	-	Trophectoderm
	10	74769431	-	Tissue (5/5)
	10	74887471	-	Tissue (5/5)
	11	71288843	+	Tissue (5/5)
	13	4312326	-	Trophectoderm
	13	60099214	+	Tissue (5/5)
	13	60286044	+	Tissue (5/5)
	14	3292456	-	Tissue (5/5), Trophectoderm
	14	105938355	+	Tissue (5/5)
	14	106091074	+	Tissue (5/5), Trophectoderm
15	68869794	+	Trophectoderm	
15	110500242	+	Tissue (5/5)	
16	23922930	+	Tissue (5/5)	
17	28273860	-	Trophectoderm	
19	52268724	-	Trophectoderm	
X	10162792	-	Trophectoderm	
X	70629586	+	Trophectoderm	
X	144392412	+	Trophectoderm	

\*Five tissue biopsies were taken—axillary lymph node, liver, muscle, rectum, and skin.

health, alanine transaminase (27 to 80 IU/L, normal range 18.9 to 94.2 IU/L), and total bilirubin (0.08 to 0.15 mg/dL, normal range 0 to 0.4 mg/dL), remained within normal limits. Thus, both Tauro and Cholie appear completely healthy as compared to other rhesus macaques in the same colony.

**Confirmation of HBV Pre-S1 Binding to hNTCP In Vivo.** While hNTCP RNA expression in the livers of Tauro and Cholie was promising, additional validation was required to demonstrate HBV pre-S1 binding to hNTCP in vivo, a critical step in HBV hepatocyte entry. We intravenously infused 0.3 mg/kg of MyrB conjugated to the fluorophore indocyanine green (ICG) into Tauro, Cholie, and a nontransgenic rhesus macaque (RM 5) and measured fluorescence in the liver 40 h later using a fluorescence imaging laparoscope. The timing of this imaging was based on previously published SPECT/CT data showing radiolabeled MyrB binding in beagle livers for up to 48 h, while the signal in cynomolgus macaque livers was lost within 24 h (31). We found that Tauro and Cholie exhibited diffuse liver fluorescence, indicating a specific binding of MyrB-ICG to the liver cells, while the nontransgenic animal showed minimal liver fluorescence (Fig. 3A). Images from all three animals revealed an increased fluorescent signal in the gallbladder, likely due to normal buildup of ICG in the gallbladder during biliary clearance (32).

Quantification of the corrected fluorescence signal revealed that compared to the nontransgenic animal, Tauro's liver had a 6.02-fold and Cholie's liver had a 10.15-fold greater signal intensity, respectively (Fig. 3B). These data demonstrated that hNTCP binds to HBV pre-S1 in transgenic rhesus macaque livers.

**HBV Infection of hNTCP Transgenic PH.** We have previously demonstrated that isolated rhesus macaque PH cannot support HBV infection. However, when these PH express hNTCP either via adenovirus or adeno-associated virus (AAV) transduction, they can support the entire HBV life cycle (29). Therefore, we next interrogated whether PH from our transgenic animals were permissive to HBV infection. Due to the advanced age and higher body weight of Tauro compared to Cholie, we performed a laparoscopic liver partial lobectomy with Tauro and isolated PH. We then infected these PH with a highly sensitive reporter HBV (MOI = 250 genomic equivalents/cell) expressing and secreting NanoLuc luciferase (HBV-NanoLuc). Efficient in vitro infection of PH with HBV requires the inclusion of polyethylene glycol (PEG), which is believed to improve the initial binding of HBV to the cell surface (33). Given the unknown ramifications of endogenously expressed hNTCP on rhesus macaque PH, HBV-NanoLuc infections were performed in both the presence

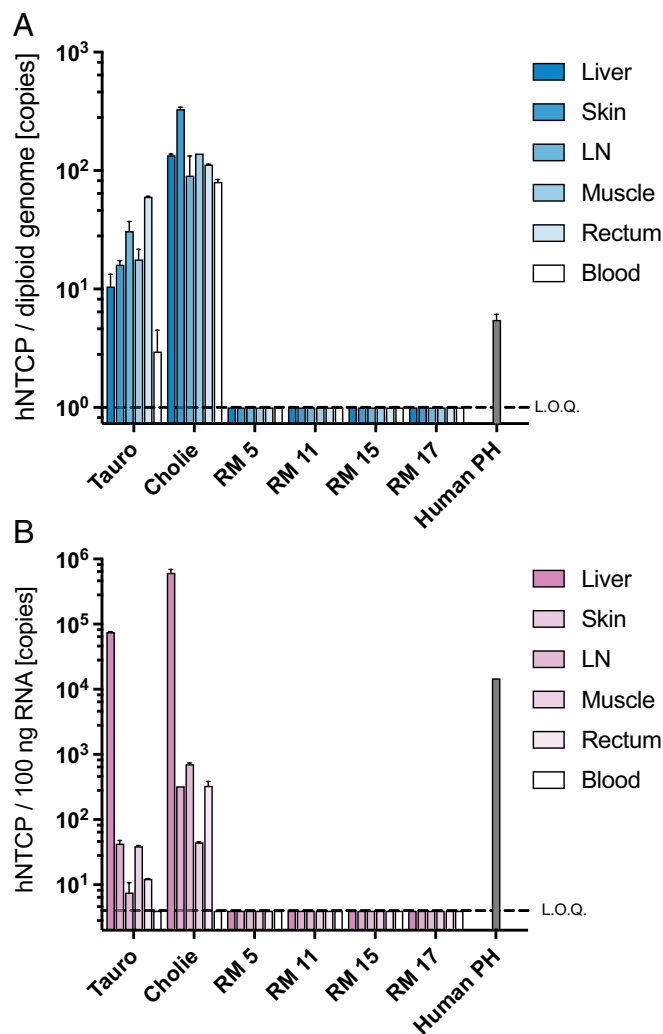


**Fig. 2.** Testing of multiple tissues for hNTCP integration and expression. (A) hNTCP DNA quantification in the liver, skin, axillary lymph node (LN), muscle, and rectum of transgenic infants Tauro and Cholie compared to nontransgenic rhesus macaques and human PH. (B) hNTCP RNA quantification for the same animals and tissues as panel A.

and absence of PEG. In addition, to confirm that the infection of Tauro's PH with HBV-NanoLuc was facilitated through the hNTCP receptor, we also tested blocking the receptor with MyrB prior to infection. We collected supernatants between one- and five-days post-infection (dpi) and found that Tauro's PH secreted high levels of NanoLuc following infection with HBV-NanoLuc (an average 1,059-fold increase from baseline on 5 dpi) (Fig. 4A). In line with previous reports (33), we found that removal of PEG from the media significantly reduced the magnitude of infection. However, given the sensitivity of the NanoLuc assay, we still detected infection by 5 dpi (an average 24-fold increase

from baseline on 5 dpi) (Fig. 4A). Finally, we were able to block infection of PH by treatment with MyrB, indicating that the infection is contingent on the expression and HBV Pre-S1 binding of the hNTCP transgene (Fig. 4A).

Having shown infection with the HBV-NanoLuc reporter virus, we next aimed to determine whether Tauro's PH were susceptible to replication-competent wild-type HBV. We performed a similar infection experiment using the commonly utilized lab strain HBV genotype D serotype ayw (MOI = 500 genome equivalents/cell). We found secreted hepatitis B "e" and surface antigens (HBeAg and HBsAg) in the supernatant, which was not detected in similarly infected nontransgenic PH (Fig. 4B). In addition, intracellular HBV DNA and RNA were found in Tauro's HBV-infected PH (Fig. 4C). These data show that Tauro's PH also supported wild-type HBV infection, as HBeAg, HBsAg, and high levels of intracellular HBV RNA were all detected (Fig. 4B and C). MyrB blocking prevented infection with HBV, as analysis of supernatants from Tauro's PH had undetectable antigen levels and cellular HBV RNA was reduced 10,000-fold (Fig. 4B and C). HBV DNA was detectable at 3 dpi regardless of MyrB blocking, indicating remaining HBV inoculum (Fig. 4C). However, HBV DNA increased only in the unblocked infection, demonstrating HBV genome replication. Finally, we stained Tauro's HBV-infected PH for expression of HBsAg and analyzed the cells by fluorescent microscopy, which showed cytoplasmic expression of HBsAg only in PH without MyrB blocking (SI Appendix, Fig. S3). Taken together, these data conclusively confirm that the hNTCP transgene facilitates HBV entry and show that PH from Tauro are susceptible to HBV infection.

## Discussion

Germline genetic engineering of nonhuman primates using lentiviral vectors was first reported in 2001 (7). However, only a handful of transgenic nonhuman primates have been created since, nearly all using lentiviral and CRISPR/Cas technologies (4). Here, we utilized the injection of DNA transposons and PB mRNA into fertilized zygotes to generate the first transgenic nonhuman primate model for infectious disease research with tissue-specific transgene expression of the HBV receptor hNTCP. Indeed, given the challenges of embryonic gene knock-in by lentiviral vectors or directed DNA repair, our method only requires a DNA plasmid and PB mRNA to achieve transgenic animals. Overall, this adaptable technique has significant advantages for creating transgenic nonhuman primates that will serve as valuable models for understanding and treating human diseases.

In addition to advancing nonhuman primate transgenic technologies, Tauro and Cholie represent an important step toward providing a currently absent immunocompetent, preclinical model to the HBV field. Current methods of inducing HBV susceptibility in rhesus macaques involve intravenous, high-dose Ad5-hNTCP infusion prior to HBV challenge, providing hepatocyte targets within the liver (29). This strategy has several drawbacks. First, the number of HBV-susceptible hepatocytes is limited by the

**Table 3. Serum chemistry profiles from Tauro and Cholie**

Animal ID	Age (weeks)	ALT (IU/L) ref range: 18.9 to 94.2	AST (IU/L) ref range: 18 to 58	ALKP (IU/L) ref range: 114 to 482	ALB (g/dL) ref range: 3.3 to 4.7	TBil (mg/dL) ref range: 0.0 to 0.4	GGT (IU/L) ref range: 35 to 72
Tauro	62.6	41	66	748	4.4	0.08	100
	72.6	68	50	190	4	0.1	45
	81	80	66	569	4	0.15	84
Cholie	31.4	27	48	1,002	4.1	0.1	134

IU = international units, ALT = alanine transaminase, AST = aspartate transaminase, ALKP = alkaline phosphatase, ALB = albumin, TBil = total bilirubin, GGT = gamma-glutamyl transferase.

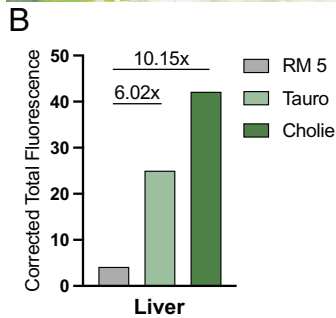
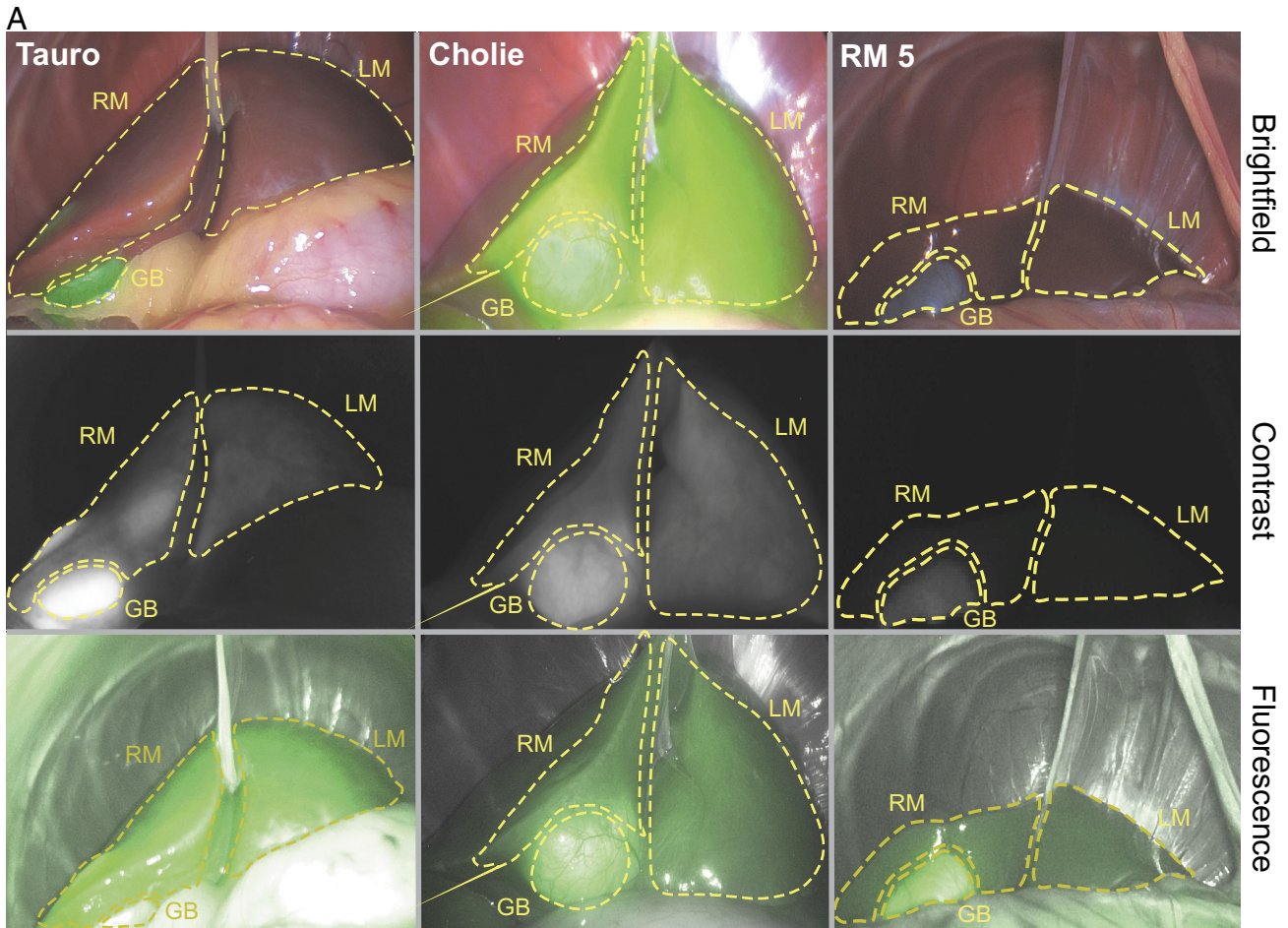


**Fig. 3.** In vivo binding of MyrB-ICG to hNTCP in the liver. (A) Brightfield, contrast, and fluorescent images of Tauro (Left), Cholie (Center), and nontransgenic control RM 5 (Right). (B) Quantification of ICG fluorescence following correction for background.

transduction efficiency of Ad5-hNTCP. Second, transduction with Ad5-hNTCP results in transient expression due to the loss of episomal adenoviral genomes during cellular division. Finally, Ad5-hNTCP is immunogenic and may confound HBV replication dynamics. Tauro and Cholie alleviate all these drawbacks since hepatocytes express the hNTCP transgene from the genome and vector-mediated transduction is not required. Indeed, isolated PH from Tauro showed HBV susceptibility, setting the stage for future in vivo infections of future offspring.

To fully realize the potential of this model, we must increase the number of hNTCP transgenic rhesus macaques by using Tauro and Cholie as the foundation for breeding. Although our data from various tested tissues strongly suggests that the monkeys are not mosaics, this cannot be definitively confirmed until various cell types are tested at the single-cell level. In addition, we cannot definitively state that hNTCP integrants will be transmitted in the germline of these animals. Tauro and Cholie are expected to

reach sexual maturity in 2025, at which point we will begin collecting gametes to confirm the transgene in their germlines and use them for IVF. Given the high number of integrants found in Cholie, it is highly likely that her eggs will harbor the transgene, making her a suitable founder animal. However, we do not know which of the multiple integrations actively express hNTCP, necessitating further functional analysis of the offspring. In contrast, the single integrant found in Tauro will presumably lead to functional expression, but only in 50% of his offspring, necessitating genetic analysis of IVF-derived embryos. Since Tauro and Cholie are half-siblings (Table 1), we will use additional wild-type rhesus macaques for breeding purposes to increase genetic diversity.

Overall, our rhesus macaque model of HBV infection will be critical to the study of pathogenesis, immunity, and therapeutic strategies. It will also allow us to model the perinatal vertical transmission of HBV from mother-to-child, which is responsible for most chronic infections worldwide (24). Given the high success

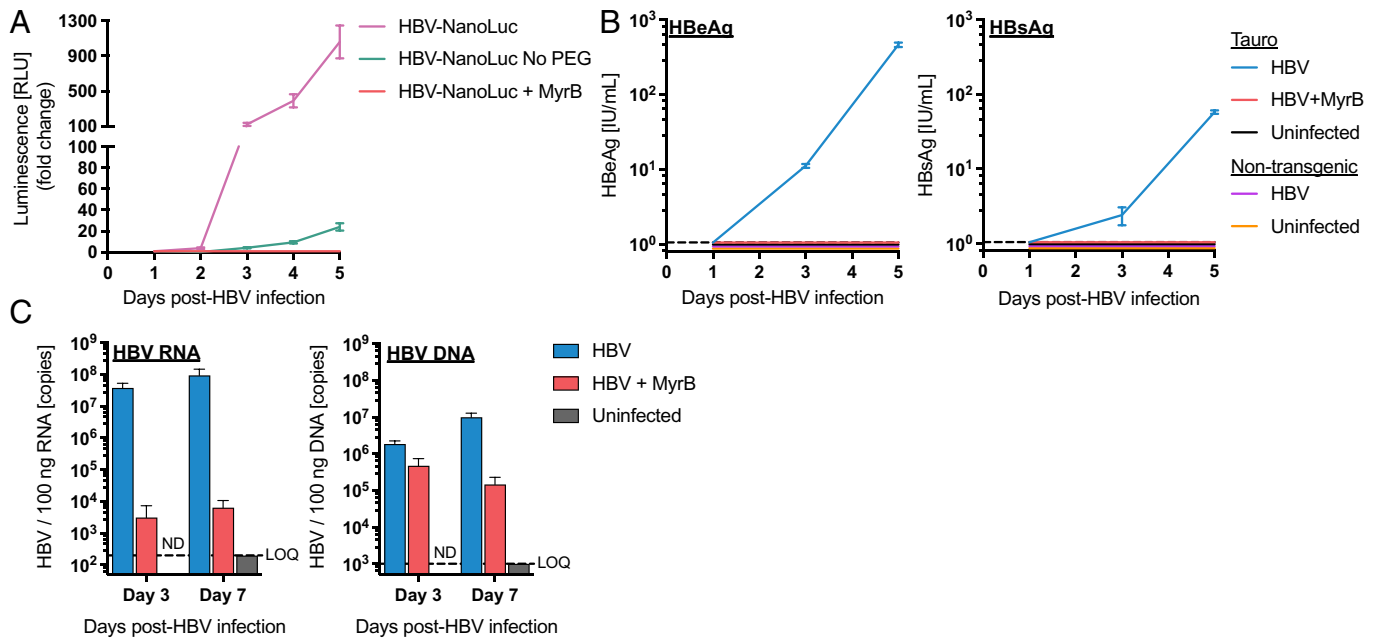


**Fig. 4.** PH from Tauro are susceptible to HBV infection. (A) Luminescence measurements from supernatants of HBV-NanoLuc infected PH. (B) HBeAg and HBsAg concentrations in supernatants of wildtype HBV-infected PH. (C) Quantification of total cellular HBV RNA and DNA from HBV-infected PH.

rate of in vitro-derived pregnancies at our center, research and breeding can be supported over the next several years until a larger colony can more fully supply the needs of HBV researchers internationally.

## Methods

**PB Transposon Vector.** PB transposon plasmid PB511B-1 (System Biosciences, LLC) was digested with restriction enzymes *SpeI* and *CsiI* and the transposon backbone was gel purified. An expression cassette containing the TTR promoter, human *SLC10A1* (hNTCP), WPRE, and a bovine growth hormone polyA tail was amplified with primers containing the *SpeI* and *CsiI* restriction sites, purified, and digested with restriction enzymes *SpeI* and *CsiI*. This cassette was then ligated into the transposon backbone with T4 ligase.

**Animals.** All rhesus macaques used in this study were cared for in adherence with the guidelines set forth by the Office of Laboratory Animal Welfare at the Oregon National Primate Research Center, which maintains accreditation with the Association for Assessment and Accreditation of Laboratory Animal Care. Procedures were conducted in strict accordance with Institutional Animal Care and Use Committee approved protocol TR02\_IPO0001110 and carried out by trained veterinarians and technical staff.

**Gamete Collection and IVF.** As detailed previously, sexually mature female rhesus macaques with regular ovarian cyclicity underwent a standard eight-day controlled ovary stimulation protocol to produce multiple preovulatory follicles (34, 35). Beginning two to four days after observation of menstrual bleeding, 30 IU of recombinant, human-FSH (r-hFSH) was administered intramuscularly twice daily for days 1 to 8 of the controlled ovarian stimulation protocol. On days 7 and 8, 30 IU of luteinizing hormone was added to the r-hFSH injections to support continued follicle development. Estradiol-17 $\beta$  (E2) and progesterone (P4) blood serum levels were assayed by immunochemiluminescence every other day by the Oregon National Primate Research Center Endocrine Technology Core on a Roche Cobas immunoassay platform to confirm increasing estradiol (growing follicles). When circulating E2 levels reached 200 pg/mL or greater, 0.075 mg/kg of the gonadotropin releasing hormone antagonist Acyline was given intramuscularly to prevent an endogenous luteinizing hormone surge. On day 8 of the protocol, 1,100 IU of human chorionic gonadotropin (hCG) was given subcutaneously to trigger ovulatory events in the ovary and meiosis resumption in the oocytes. Between 34 to 36 h after hCG, follicles were aspirated by percutaneous ultrasound

guidance or laparoscope, and oocytes were recovered and sorted. Mature MII stage ova with a clearly visible polar body in the perivitelline space were selected for IVF. Sexually mature male rhesus macaques with proven fertility underwent penile stimulation and semen collection the same day as the oocyte recovery to collect semen as previously described (34, 35). Semen samples were washed in HEPES-buffered TALP medium (34), and concentration and motility were determined by computer assisted sperm analysis (36). Postretrieval ova were stripped free of surrounding cumulus cells and inseminated with 1  $\mu$ L of activated sperm (2 million/mL) in a 100  $\mu$ L drop of BO-IVF medium (IVF Bioscience, Cat# 61003) under oil and incubated at 37  $^{\circ}$ C in 5% CO<sub>2</sub> humidified air for 14 to 16 h. Any remaining sperm attached to the zona pellucida were removed by gentle pipetting, and ova were observed for the presence of either 2 polar bodies or 2 pronuclei, indicating fertilization and formation of a zygote stage embryo.

**Embryo Microinjection and Trophectoderm Biopsy.** Identified zygotes were stabilized on a glass holding pipette by suction and injected into both pronuclei (when present) and the cytoplasm under continuous flow with 10 to 100 pL of editing material. Editing material consisted of 30 ng/ $\mu$ L PB mRNA (Hera BioLabs, Cat# SPB-100) and 95 ng/ $\mu$ L transposon DNA plasmid suspended in injection buffer consisting of 10 mM Tris-HCl (ThermoFisher, Cat# J60636.K2) and 0.1 mM EDTA (ThermoFisher, Cat# AM9260G) in nuclease-free water (ThermoFisher, Cat# AM9932). The embryos were then washed into fresh BO-IVC medium (IVF Bioscience, Cat# 61001) and cultured at 37  $^{\circ}$ C for 7 to 8 d to the blastocyst stage in a trigas mixture of 5% CO<sub>2</sub>/6% O<sub>2</sub>/89% N<sub>2</sub> in humidified air.

To recover embryonic cells for genetic analysis, expanded blastocysts were stabilized similar as with microinjections, and an objective mounted laser (Hamilton Thorne, Beverly, MA) was used to dissect approximately 10 cells from the trophectoderm. The dissected cells were snap-frozen for genotyping and the collapsed blastocyst was immediately cryopreserved using the global<sup>®</sup> Blastocyst Fast Freeze kit (Cooper Surgical, Cat# GFT5-005), as per the manufacturer's instructions, in 0.25 cc straws, and stored in liquid nitrogen.

**Embryo Transfer.** Embryos possessing the integrated hNTCP gene were thawed using the global<sup>®</sup> Blastocyst Fast Freeze Thawing kit (Cooper Surgical, Cat# GFT5-055), as per the manufacturer's instructions, and allowed to recover in BO-IVC for 2 h at 37  $^{\circ}$ C in a trigas mixture of 5% CO<sub>2</sub>/6% O<sub>2</sub>/89% N<sub>2</sub> in humidified air before transfer into a recipient. Embryo recipients were tracked through a natural menstrual cycle by daily serum E2 and P4 measurements, beginning on day 7 post observation of menses, to detect ovulation. Recovered blastocysts were loaded into a transfer catheter in 10  $\mu$ L of HEPES-buffered TALP. The tip of

the catheter was inserted into the fimbria surrounding the ovary with an ovulated follicle via laparotomy and passed approximately 3 cm into the ampulla region of the fallopian tube to place the embryo(s) into recipients that were day 3 or 4 of the luteal phase, postovulation as defined by E2 peak. Up to two blastocysts were transferred into a recipient each time. Recipient animals were checked 30 d after the transfer by ultrasound to determine whether implantation occurred. On occasions when recipients were naturally timed to blastocysts developing in culture, embryos were transferred fresh. Six total pregnancies were generated utilizing this method generating five healthy singletons and one set of twins, Table 1.

**hNTCP DNA and RNA Quantification.** Total cellular DNA and RNA were extracted from tissues using the AllPrep DNA/RNA Kit according to the manufacturer's instructions (Qiagen Cat# 80284). hNTCP DNA and RNA were quantified via qPCR as described elsewhere (29).

**Enhanced-Specificity Tagmentation-Assisted (esTag)-PCR.** Trophectoderm biopsy DNA was extracted as previously described (30). Transgene integration location and copy number were determined by esTag-PCR from total cellular DNA from trophectoderm and tissue biopsies as described elsewhere (30). To account for sequencing artifact, only integrations where >2% of aligned sequencing reads matched the same genomic location are reported.

**Sanger Sequencing.** Targeted sequencing was performed following PCR amplification of the presumed hNTCP insertion sites (based on esTag-PCR data) from liver biopsy DNA. Primer sets were designed using one of two universal, inverted terminal repeat-specific primers for the 5' (CAGACCGATAAACACATGCGTCA) and 3' (AGCGACGGATTCGCGCTATT) ends, along with genomic primers (variable sequence, *SI Appendix, Table S2*). A three-step PCR cycling protocol was used with an annealing temperature of 62 °C. Each PCR reaction included DNA template (5 ng), 1 × KAPA HiFi HotStart ReadyMix (Roche, Cat# KK2602), primers (400 nM each), and 5% DMSO. PCR products were isolated via gel electrophoresis in 1% agarose and purified using QIAquick Gel Extraction Kit (Qiagen, Cat# 28704). Purified PCR products were quantified using the Qubit dsDNA Broad Range Kit (ThermoFisher Scientific, Cat# Q32850) on a Qubit 4.0 Spectrophotometer. Purified PCR products were shipped to Eurofins Genomics, Inc. for Sanger sequencing. Resultant sequences were analyzed using SnapGene and determination of transgene integration number and location are detailed in *SI Appendix, Table S1*.

**Fluorescence Imaging Using ICG-Conjugated MyrB.** Rhesus macaques received an intravenous injection of 0.3 mg/kg ICG-conjugated MyrB (GTNLSVP NPLGFFPDHQLDPAFGANSNNPDWFNPNKDHWPENKVGCG-[ICG]) followed 40 h later by fluorescence imaging using a Stryker 1688 laparoscopy unit. A 5 mm telescope was placed through a midline incision caudal to the umbilicus followed by visualization of the liver and imaging. Image quantification was performed using ImageJ software where a region of interest in the contrast image was selected and fluorescence measured using the software. Next, a nonfluorescent region was selected as background and fluorescence was measured using the software. This process was iterated until all regions of interest were selected and Results measured by the software. The corrected total cell fluorescence (CTCF) was calculated using the following equation:  $CTCF = \text{Integrated Density} - (\text{Area of Region of Interest} \times \text{Mean Fluorescence of Background Readings})$  (37).

**Laparoscopic Liver Partial Lobectomy.** An approximately 2/3 partial lobectomy of the left lateral lobe of the liver was performed as described previously (38, 39) with the following changes to permit the larger sample collection through three 5 mm ports. The rhesus macaque was in dorsal recumbency, the camera port was placed caudal to the umbilicus and the two midabdominal instrument ports were placed approximately 2 to 3 cm off midline on each side. A Caiman 5 Vessel Sealer was used to perform the partial lobectomy followed by removal of the liver tissue from the abdomen in a tissue bag to avoid damaging the sample.

**Isolation of Rhesus Macaque PH.** The biopsied left lateral liver lobe was placed in a petri dish and a catheter (Introcan Safety 20G IV Catheter, Cat# 4251644) was inserted into the exposed vein and adhered using surgical glue. Tubing that had been flushed with Pre-Perfusion Media consisting of HBSS<sup>-/-</sup> (Fisher Scientific, Cat# MT21021CV), 0.1% 0.5 M EGTA (Bioworld, Cat# 40520008), 0.5% 10 IU/mL Heparin (NDC# 63323-540-33) was attached to the catheter and fed through

a Masterflex L/S Easy-Load peristaltic pump (ColePalmer, Cat# 77200-50). The other end of the tubing was placed in a beaker containing Pre-Perfusion Media, and the pump was turned on at a rate of 40 mL/min, with the media perfused through the lobe into the petri dish being aspirated during the process. Once 250 mL of Pre-Perfusion Media had been pumped through the lobe, the tubing was moved to a new beaker containing 250 mL HBSS<sup>+/+</sup> (ThermoFisher, Cat# 24020117). The pump was turned on at a flow rate of 40 mL/min, and once all 250 mL of HBSS<sup>+/+</sup> was pumped through the lobe, the pump was turned off. Then, 150 mL Collagenase Base Buffer (HBSS<sup>+/+</sup>, 1.5% heat-inactivated fetal bovine serum (NeuroMics, Cat# FBS002), 0.2% 1M CaCl<sub>2</sub> (Sigma Aldrich, Cat# 21115), and 0.5% 1M HEPES (Thermo Fisher, Cat# SH30237.01) was added to the beaker and placed in a 37 °C water bath. The pump was turned on at a rate of 40 mL/min and once 50 mL of Collagenase Base Buffer was pumped through the lobe, the pump was stopped and 25 mg NB4 Collagenase (Crescent Chemical, Cat# 17465) was added to the beaker. The liver lobe was removed from the petri dish and placed in the beaker containing the Collagenase Buffer Solution to create a closed-loop system. The pump was turned on at a rate of 40 mL/min for 40 min. After incubation, the liver was removed from the water bath, gently probed with forceps, and dissected with scalpels. The liver solution was filtered through a 100- $\mu$ m filter, and the filtrate was centrifuged at 50 × g for 3 min. The pellet was washed twice in Cell Culture Media consisting of DMEM-F12 (Fisher Scientific, Cat# 11-320-082), 10% heat-inactivated fetal bovine serum (NeuroMics, Cat# FBS002), 1% antibiotic/antimycotic solution (Fisher Scientific, Cat# SV30079.01), 1% L-Glutamine (ThermoFisher, Cat# 25030081), and 1% sodium pyruvate (Fisher Scientific, Cat# SH3023901), and then centrifuged at 50 × g for 3 min. The pellet was resuspended in Cell Culture Media and filtered through a 70- $\mu$ m filter then centrifuged at 50 × g for 3 min. Finally, the hepatocytes were resuspended in Cell Culture Media, quantified, and used for further experiments.

**Generation of HBV and HBV-NanoLuc.** HBV and HBV-NanoLuc particles were purified by heparin affinity chromatography and sucrose density ultracentrifugation from the supernatant of stable producer cells as previously described (40). HepAD38 were used to secrete HBV and a HepG2-NTCP-K7-based HBV producer cell clone to secrete HBV-NanoLuc (41, 42). The HepG2-HBV-NanoLuc producer cell clone was generated by two rounds of transfection followed by cell clone selection. First, a helper cell clone for HBV-NanoLuc packaging was generated by transfecting HepG2-NTCP-K7 cells with a plasmid encoding a TTR promoter followed by a truncated HBV genotype D genome (2259 to 1842 bp) (GeneBank, Accession# MF967563), an internal ribosomal entry site, a puromycin N-acetyltransferase gene, and a bovine growth hormone polyadenylation signal, followed by puromycin selection. This helper cell clone was then transfected with a plasmid encoding a G418 selection cassette and the genotype D HBV genome harboring a TTR-NanoLuc expression cassette inserted in the surface protein open reading frame as previously described (43) and selected with G418.

**Infection of PH with HBV-NanoLuc and HBV.** PH were plated at a density of  $1 \times 10^6$  cells/well on cell culture-treated flat-bottom microplates (Fisher Scientific, Cat# 08-772-3) coated with rat-tail collagen at 300  $\mu$ g/mL (Fisher Scientific, Cat# A1048301). PH used for HBV-NanoLuc and HBV infection were plated in PH Media (Cell Culture Media with 2% DMSO, Sigma Cat# D2438). After 24 h in culture, MyrB (LifeTein, Cat# 36511) was added to relevant wells at 1  $\mu$ M prior to infection with HBV-NanoLuc or wt-HBV (MOI = 250) in Infection Media consisting of Cell Culture Media with 4% PEG6000 (Sigma, Cat# 81253) and 2% DMSO. Supernatants were collected post-infection and media were replaced with PH Media. On days 3 and 7 post-HBV, PH were lysed for HBV DNA and RNA quantification.

**HBV-NanoLuc Quantification.** Luciferase activity on supernatants was determined 1, 2, 3, 4, and 5 d post HBV-NanoLuc infection as described elsewhere (44).

**HBsAg and HBeAg Detection by Chemiluminescent Immunoassay (CLIA).** HBsAg and HBeAg detection by CLIA. HBsAg and HBeAg supernatant concentrations were determined using the Hepatitis B Surface Antigen (Ig Biotech, Cat# CL18003) and Hepatitis B Virus (HBV) "e" Antigen CLIA kits (Ig Biotech, Cat# CL18005) according to the manufacturer's instructions. Samples were processed and analyzed as described elsewhere (29).

**HBV DNA and RNA Extraction and Quantification.** Total cellular RNA and DNA were extracted using the AllPrep DNA/RNA Kit according to the manufacturer's instructions (Qiagen, Cat# 80284). RNA and DNA were quantified via qPCR as described elsewhere (29).

**Microscopy of HBV-Infected PH.** On day 7 post-HBV infection, PH were washed once with 1 × PBS and then fixed with 4% paraformaldehyde (Fisher Scientific, Cat# 50-980-495) at 25 °C for 10 min. PH were washed twice with 1 × PBS then permeabilized with 0.2% Triton X-100 (Sigma Aldrich, Cat# X100) at 25 °C for 15 min. PH were washed twice with 1 × PBS then stained with mouse IgG2b α-HBs (Biolegend, Cat# 932302) diluted 1:250 in 1 × PBS at 25 °C for one hour. PH were washed twice with 1 × PBS then stained with AlexaFluor594-conjugated α-mouse IgG (H + L) secondary antibody (Invitrogen, Cat# A21203) diluted 1:250 in 1 × PBS at 25 °C for one hour. PH were then washed twice with 1 × PBS then stained with DAPI (Invitrogen, Cat# D1306) diluted 1:10,000 in TBS-T at 25 °C for 10 min. PH were washed twice with 1 × PBS and then visualized on a BZ-X810 Series Keyence Fluorescence Microscope.

**Data, Materials, and Software Availability.** Primary data and images data have been deposited in FigShare (<https://doi.org/10.6084/m9.figshare.27905898>) (45). All study data are included in the article and/or *SI Appendix*.

**ACKNOWLEDGMENTS.** We thank the veterinary and animal care staff for their contributions to this study. This work was supported by NIH Grants R21 AI133632 (B.J.B.), R01 AI157612 (B.J.B.), DP1 DA056493 (J.O.L.), and P51 OD011092 (ONPRC).

Author affiliations: <sup>a</sup>Division of Pathobiology and Immunology, Oregon National Primate Research Center, Oregon Health and Science University, Beaverton, OR 97006; <sup>b</sup>Institute of Virology, Technical University of Munich/Helmholtz Munich, Munich 81675, Germany; <sup>c</sup>German Center for Infection Research, Munich Partner Site, Munich 81675, Germany; <sup>d</sup>Division of Reproductive and Developmental Sciences, Oregon National Primate Research Center, Oregon Health and Science University, Beaverton, OR 97006; <sup>e</sup>Division of Comparative Medicine, Oregon National Primate Research Center, Oregon Health and Science University, Beaverton, OR 97006; <sup>f</sup>Division of Genetics, Oregon National Primate Research Center, Oregon Health and Science University, Beaverton, OR 97006; and <sup>g</sup>Division of Metabolic Health and Disease, Oregon National Primate Research Center, Oregon Health and Science University, Beaverton, OR 97006

1. J. Xu *et al.*, Gene editing in rabbits: Unique opportunities for translational biomedical research. *Front. Genet.* **12**, 642444 (2021), 10.3389/fgene.2021.642444.
2. H. T. L. Phan, K. Kim, H. Lee, J. K. Seong, Progress in and prospects of genome editing tools for human disease model development and therapeutic applications. *Genes (Basel)* **14**, 483 (2023), 10.3390/genes14020483.
3. F. Gao *et al.*, Advances and applications of genetically modified pig models in biomedical and agricultural field. *Yi Chuan* **45**, 6–28 (2023), 10.16288/j.ycz.22-313.
4. W. Liang *et al.*, Gene editing monkeys: Retrospect and outlook. *Front. Cell Dev. Biol.* **10**, 913996 (2022), 10.3389/fcell.2022.913996.
5. J. E. Park, A. C. Silva, Generation of genetically engineered non-human primate models of brain function and neurological disorders. *Am. J. Primatol.* **81**, e22931 (2019), 10.1002/ajp.22931.
6. K. Sato, E. Sasaki, Genetic engineering in nonhuman primates for human disease modeling. *J. Hum. Genet.* **63**, 125–131 (2018), 10.1038/s10038-017-0351-5.
7. A. W. S. Chan, K. Y. Chong, C. Martinovich, C. Simerly, G. Schatten, Transgenic monkeys produced by retroviral gene transfer into mature oocytes. *Science* **291**, 309–312 (2001), 10.1126/science.291.5502.309.
8. E. Sasaki *et al.*, Generation of transgenic non-human primates with germline transmission. *Nature* **459**, 523–527 (2009), 10.1038/nature08090.
9. Y. Niu *et al.*, Transgenic rhesus monkeys produced by gene transfer into early-cleavage-stage embryos using a simian immunodeficiency virus-based vector. *Proc. Natl. Acad. Sci. U.S.A.* **107**, 17663–17667 (2010), 10.1073/pnas.1006563107.
10. Y. Seita *et al.*, Generation of transgenic cynomolgus monkeys that express green fluorescent protein throughout the whole body. *Sci. Rep.* **6**, 24868 (2016), 10.1038/srep24868.
11. Y. Seita *et al.*, Generation of transgenic cynomolgus monkeys overexpressing the gene for amyloid-beta precursor protein. *J. Alzheimers Dis.* **75**, 45–60 (2020), 10.3233/JAD-191081.
12. Z. Liu *et al.*, Autism-like behaviours and germline transmission in transgenic monkeys overexpressing MeCP2. *Nature* **530**, 98–102 (2016), 10.1038/nature16533.
13. S. H. Yang *et al.*, Towards a transgenic model of Huntington's disease in a non-human primate. *Nature* **453**, 921–924 (2008), 10.1038/nature06975.
14. Y. Niu *et al.*, Early Parkinson's disease symptoms in alpha-synuclein transgenic monkeys. *Hum. Mol. Genet.* **24**, 2308–2317 (2015), 10.1093/hmg/ddu748.
15. S. Wang *et al.*, Generation of transgenic sperm expressing GFP by lentivirus transduction of spermatogonial stem cells in vivo in cynomolgus monkeys. *Vet. Sci.* **10**, 104 (2023), 10.3390/vetsci10020104.
16. M. J. Wolfgang *et al.*, Rhesus monkey placental transgene expression after lentiviral gene transfer into preimplantation embryos. *Proc. Natl. Acad. Sci. U.S.A.* **98**, 10728–10732 (2001), 10.1073/pnas.181336098.
17. H. Wan *et al.*, One-step generation of p53 gene biallelic mutant cynomolgus monkey via the CRISPR/Cas system. *Cell Res.* **25**, 258–261 (2015), 10.1038/cr.2014.158.
18. Y. Zhou *et al.*, Atypical behaviour and connectivity in SHANK3-mutant macaques. *Nature* **570**, 326–331 (2019), 10.1038/s41586-019-1278-0.
19. X. Yao *et al.*, Generation of knock-in cynomolgus monkey via CRISPR/Cas9 editing. *Cell Res.* **28**, 379–382 (2018), 10.1038/cr.2018.9.
20. S. M. Mathew, Strategies for generation of mice via CRISPR/HDR-mediated knock-in. *Mol. Biol. Rep.* **50**, 3189–3204 (2023), 10.1007/s11033-023-08278-8.
21. N. Sandoval-Villegas, W. Nurieva, M. Amberger, Z. Ivics, Contemporary transposon tools: A review and guide through mechanisms and applications of Sleeping Beauty, piggyBac and Tol2 for genome engineering. *Int. J. Mol. Sci.* **22**, 5084 (2021), 10.3390/ijms22105084.
22. A. Lacoste, F. Berenshteyn, A. H. Brivanlou, An efficient and reversible transposable system for gene delivery and lineage-specific differentiation in human embryonic stem cells. *Cell Stem Cell* **5**, 332–342 (2009), 10.1016/j.stem.2009.07.011.
23. K. Woljten *et al.*, piggyBac transposition reprograms fibroblasts to induced pluripotent stem cells. *Nature* **458**, 766–770 (2009), 10.1038/nature07863.
24. World Health Organization. Hepatitis B factsheet. <http://www.who.int/mediacentre/factsheets/fs204/en/> (2022).
25. J. Ye, J. Chen, Interferon and hepatitis B: Current and future perspectives. *Front. Immunol.* **12**, 733364 (2021), 10.3389/fimmu.2021.733364.
26. Y. C. Wang *et al.*, Predictors of response to pegylated interferon in chronic hepatitis B: A real-world hospital-based analysis. *Sci. Rep.* **6**, 29605 (2016), 10.1038/srep29605.
27. S. F. Müller, A. König, B. Döring, D. Glebe, J. Geyer, Characterisation of the hepatitis B virus cross-species transmission pattern via Na+/taurocholate co-transporting polypeptides from 11 New World and Old World primate species *PLoS ONE* **13**, e0199200 (2018), 10.1371/journal.pone.0199200.
28. B. J. Burwitz *et al.*, Hepatocytic expression of human sodium-taurocholate cotransporting polypeptide enables hepatitis B virus infection of macaques. *Nat. Commun.* **8**, 2146 (2017), 10.1038/s41467-017-01953-y.
29. S. Biswas *et al.*, Long-term hepatitis B virus infection of rhesus macaques requires suppression of host immunity. *Nat. Commun.* **13**, 2995 (2022), 10.1038/s41467-022-30593-0.
30. J. Ryu *et al.*, Rapid, accurate mapping of transgene integration in viable rhesus macaque embryos using enhanced-specificity tagmentation-assisted PCR. *Mol. Ther. Methods Clin. Dev.* **24**, 241–254 (2022), 10.1016/j.omtm.2022.01.009.
31. A. Schieck *et al.*, Hepatitis B virus hepatotropism is mediated by specific receptor recognition in the liver and not restricted to susceptible hosts. *Hepatology* **58**, 43–53 (2013), 10.1002/hep.26211.
32. A. De Gasperi, E. Mazza, M. Prosperi, Indocyanine green kinetics to assess liver function: Ready for a clinical dynamic assessment in major liver surgery? *World J. Hepatol.* **8**, 355–367 (2016), 10.4254/wjh.v8.i7.355.
33. A. Schulze, P. Gripon, S. Urban, Hepatitis B virus infection initiates with a large surface protein-dependent binding to heparan sulfate proteoglycans. *Hepatology* **46**, 1759–1768 (2007), 10.1002/hep.21896.
34. C. Ramsey, C. Hanna, In vitro culture of rhesus macaque (*Macaca mulatta*) embryos. *Methods Mol. Biol.* **2066**, 341–353 (2019), 10.1007/978-1-4939-9566-0\_23.
35. N. Piekarski *et al.*, A comparison of oocyte retrieval between ultrasound-guided and laparoscopic oocyte retrieval in rhesus macaques. *Animals (Basel)* **13**, 3017 (2023), 10.3390/ani13193017.
36. F. M. De Carvalho *et al.*, Cryopreservation and preparation of thawed spermatozoa from rhesus macaques (*Macaca mulatta*) for in vitro fertilization. *J. Am. Assoc. Lab. Anim. Sci.* **60**, 396–406 (2021), 10.30802/AALAS-JAALAS-20-000028.
37. C. A. Schneider, W. S. Rasband, K. W. Eliceiri, NIH Image to ImageJ: 25 years of image analysis. *Nat. Methods* **9**, 671–675 (2012), 10.1038/nmeth.2089.
38. A. S. Zevin *et al.*, Laparoscopic technique for serial collection of liver and mesenteric lymph nodes in macaques. *J. Vis. Exp.* **123**, 55617 (2017), 10.3791/55617.
39. C. Moats *et al.*, Antimicrobial prophylaxis does not improve post-surgical outcomes in SIV/SHIV-uninfected or SIV/SHIV-infected macaques (*Macaca mulatta* and *Macaca fascicularis*) based on a retrospective analysis. *PLoS ONE* **17**, e0266616 (2022), 10.1371/journal.pone.0266616.
40. J. M. Wettengel *et al.*, Rapid and robust continuous purification of high-titer hepatitis B virus for in vitro and in vivo applications. *Viruses* **13**, 1503 (2021), 10.3390/v13081503.
41. S. K. Ladner *et al.*, Inducible expression of human hepatitis B virus (HBV) in stably transfected hepatoblastoma cells: A novel system for screening potential inhibitors of HBV replication. *Antimicrob. Agents Chemother.* **41**, 1715–1720 (1997).
42. C. Ko *et al.*, Hepatitis B virus genome recycling and de novo secondary infection events maintain stable cccDNA levels. *J. Hepatol.* **69**, 1231–1241 (2018), 10.1016/j.jhep.2018.08.012.
43. U. Protzer, M. Nassal, P. W. Chiang, M. Kirschfink, H. Schaller, Interferon gene transfer by a hepatitis B virus vector efficiently suppresses wild-type virus infection. *Proc. Natl. Acad. Sci. U.S.A.* **96**, 10818–10823 (1999), 10.1073/pnas.96.19.10818.
44. J. M. Wettengel *et al.*, High-throughput screening for the prevalence of neutralizing antibodies against human adenovirus serotype 5. *Vaccines (Basel)* **12**, 155 (2024), 10.3390/vaccines12020155.
45. L. Rust, Data from "Liver-specific transgenic expression of human NTCP in rhesus macaques confers HBV susceptibility on primary hepatocytes." Figshare. <https://doi.org/10.6084/m9.figshare.27905898>. Deposited 26 November 2024.